machines

MDPI

Article

Sensorless Speed Controller for the Induction Motor Using State Feedback and Robust Differentiators

Onofre Morfin [1,*], Fernando Ornelas-Tellez [2], Nahitt Padilla [1], Maribel Gomez [1,*], Oscar Hernandez [1], Reymundo Ramirez-Betancour [3] and Fredy Valenzuela [3]

[1] School of Electrical and Computer Engineering, Universidad Autonoma de Ciudad Juarez, Ciudad Juarez 32310, Mexico; jpadilla@uacj.mx (N.P.); al211762@alumnos.uacj.mx (O.H.)
[2] School of Electrical Engineering, Universidad Michoacana de San Nicolas de Hidalgo, Morelia 58030, Mexico; fernando.ornelas@umich.mx
[3] School of Engineering and Architecture, Universidad Juarez Autonoma de Tabasco, Villahermosa 86040, Mexico; reymundo.ramirez@ujat.mx (R.R.-B.); fredy.valenzuela@ujat.mx (F.V.)
* Correspondence: omorfin@uacj.mx (O.M.); mgomez@uacj.mx (M.G.)

Abstract

This paper introduces a novel sensorless speed control strategy for squirrel-cage induction motors, which ensures robust operation in the presence of external disturbances by applying the state feedback technique. Based on the induction motor model, the speed controller is synthesized by defining a sliding variable that is driven to zero through the supertwisting control law, ensuring the stabilization of the tracking error. The time derivative of the error variable is estimated using a robust differentiator based on the sliding-mode twisting algorithm, thereby eliminating the need to estimate the load torque. A robust observer is employed to estimate the rotor speed and flux linkages simultaneously. The convergence of the estimated rotor flux linkages is enforced through a discontinuous first-order sliding-mode input, while the convergence of the rotor speed estimate is attained via a quasi-continuous super-twisting sliding-mode input. In the proposed model, the inductance parameters are determined from the magnetizing inductance and the leakage inductances of the stator and rotor. A procedure is also presented for adjusting the stator resistance and leakage inductances, taking into account the squirrel-cage rotor type and the skin effect in alternating current conduction. The performance of the sensorless speed control system under variations in load torque and reference speed is validated through experimental testing. The rotor speed estimation provided by the robust observer is accurate. The reference speed tracking control, evaluated using a 1600–1700 rpm pulse train phase-shifted by 4 s with respect to a 0–0.5 N·m pulse train, demonstrates high precision.

Keywords: sensorless speed controller; nonlinear sliding function; sliding-mode robust observer; supertwisting robust diferentiator; inductance parameters definition

check for updates

Academic Editor: Reiko Raute

Received: 25 July 2025
Revised: 4 September 2025
Accepted: 9 September 2025
Published: 12 September 2025

Citation: Morfin, O.; Ornelas-Tellez, F.; Padilla, N.; Gomez, M.; Hernandez, O.; Ramirez-Betancour, R.; Valenzuela, F. Sensorless Speed Controller for the Induction Motor Using State Feedback and Robust Differentiators. *Machines* **2025**, *13*, 846. https://doi.org/10.3390/machines13090846

Correction Statement: This article has been republished with a minor change. The change does not affect the scientific content of the article and further details are available within the backmatter of the website version of this article.

Copyright: © 2025 by the authors. Licensee MDPI, Basel, Switzerland. This article is an open access article distributed under the terms and conditions of the Creative Commons Attribution (CC BY) license (https://creativecommons.org/licenses/by/4.0/).

1. Introduction

Induction motors have become the backbone of numerous industrial applications due to their simple construction, high reliability, and low maintenance cost. However, mechanical sensors to measure speed and torque increase system complexity and cost in high-precision control applications such as industrial robotics and high-performance servomechanisms. Sensorless control emerges as an attractive solution to eliminate these

devices, reducing maintenance, requirements, and vulnerability to sensor failures; nevertheless, it introduces the challenge of accurately estimating critical variables (speed, rotor flux, and torque), especially in the low-speed region, where current signals have small values and noise is predominant [1,2].

Recent reviews highlight the scope of modern control strategies for induction motors, from scalar and flux-oriented control to direct torque control, and their evolution through intelligent and robust algorithms [3]. Advanced approaches such as backstepping combined with high-order sliding-mode control have demonstrated improved robustness and dynamic performance in sensorless applications [4], while adaptive full-order observers and interconnected MRAS schemes have improved low-speed estimation accuracy and multiparameter identification [5,6]. MRAS-type estimators, extensively reviewed in [7], can guarantee stability across the entire speed–torque range [8] but remain sensitive to motor parameters, motivating the use of auxiliary estimators [9]. Other proposals include stator-current-based observers with rotor-flux correction and fuzzy-logic adaptation [10], neural-MRAS schemes for improved high-speed accuracy and ultra-low-speed tracking [11], and sensorless vector control for induction generators in wind systems with high-precision speed estimation [12].

Sliding-mode control (SMC) offers intrinsic robustness to parameter variations and disturbances, achieving exact decoupling of flux and torque loops once sliding motion is established [13,14]. Hybrid SMC–fuzzy logic and Lyapunov-based adaptations improve transient dynamics [15], while second-order algorithms such as the twisting method reduce chattering without sacrificing robustness [16]. Deadbeat regulators outperform proportional-integral controllers in response speed and overshoot reduction [17], while the adaptive neuro-fuzzy inference system and MRAS schemes deliver higher efficiency and shorter settling times [18]. Robust differentiators [19,20] provide strong noise rejection and finite-time convergence, making them suitable for noisy sensorless applications. Despite these advances, key challenges remain, such as ensuring asymptotic stability of observers under variable-speed and regenerative-mode conditions, achieving exact speed control in the presence of parametric uncertainties, field weakening, zero-speed operation, and low switching (minimal chattering). As previously described, sensorless speed control remains an open research area intended to achieve high dynamic performance, accurate estimation, and robustness against model parameter uncertainties.

The main contribution of this work is the synthesis of a sensorless rotor speed control system for induction motors, designed to operate with minimal parameter dependency. The proposed system integrates three robust components, (a) a rotor speed controller, (b) a rotor speed and flux linkages observer, and (c) a differentiator, each employing sliding-mode techniques in their inputs to enhance robustness. In the rotor speed controller, a novel rotor flux reference function is introduced to adjust the motor magnetization level of the induction motor according to the stator currents, which in turn depend on the load torque. This approach, to the best of our knowledge, has not been reported in the literature. Additionally, a sliding variable is designed using the linearization state feedback technique. By applying the super-twisting control law to this sliding variable, its value is driven to zero in finite time, ensuring smooth convergence of the controlled variables. In the robust observer, two complementary sliding-mode inputs are combined, another novelty of this work. A first-order discontinuous input forces the movement of a nonlinear sliding function to zero in finite time, achieving convergence of the estimated rotor flux linkages. Simultaneously, a super-twisting quasi-continuous input drives another nonlinear sliding function to zero in finite time, ensuring accurate rotor speed estimation. Finally, the robust differentiator employs the super-twisting algorithm to compute the time derivative of the tracking error variable in the presence of noise, eliminating the need for direct load-torque

measurement. The proposed methodology guarantees asymptotic stability under time-varying speed, load, and parameter uncertainties. Experimental validation confirms its high efficiency, precise estimation capability, and strong robustness.

This article is organized as follows: Section 2 introduces the squirrel-cage induction motor space–state model and the model's inductance parameter definitions; in Section 3 the synthesis of the speed controller applied to induction motor is developed; Section 4 shows the development of the speed and rotor flux observer based on first-order and supertwisting sliding modes as inputs to the system, aiming to achieve convergence in the observed variables. In Section 5 a robust differentiator is introduced from recent literature. The differentiator has the ability to deal with noisy signals. Section 6 presents experimental results to measure the performance of the open-loop speed and rotor flux observer and also the closed-loop sensorless speed controller of the induction motor.

2. Sensorless Speed Control System Methodology

The methodology for configuring the sensorless speed controller of a squirrel-cage induction motor is as follows: (a) The structure of the induction motor model is first defined and analyzed. Motor parameters are then obtained through standard tests, followed by a parameter adjustment that accounts for the squirrel-cage rotor type and incorporates the skin effect on stator resistance. This model is depicted in the box named "Induction Motor Model" of the Figure 1. (b) An observer is designed to simultaneously estimate rotor speed and rotor flux linkages. Its performance is evaluated in open-loop operations under variations in load torque and supply voltage. This observer is depicted in the box named "Robust Observer" of the same Figure. (c) The error variable $\boldsymbol{\varepsilon}_1$ is computed as the difference of the reference function $[\omega_{ref} \quad \varphi_{ref}]$ and controlled output variables ω_m and φ_r as depicted by the summation circle in Figure 1. (d) The sliding variable $\mathbf{s}^*$ is designed using the linearization state feedback technique based on the motor model structure. Additionally, control inputs are decoupled through a coordinate transformation. (e) A super-twisting control law $\mathbf{v}_s$ drives the sliding variable toward zero, ensuring smooth tracking of the error variables.

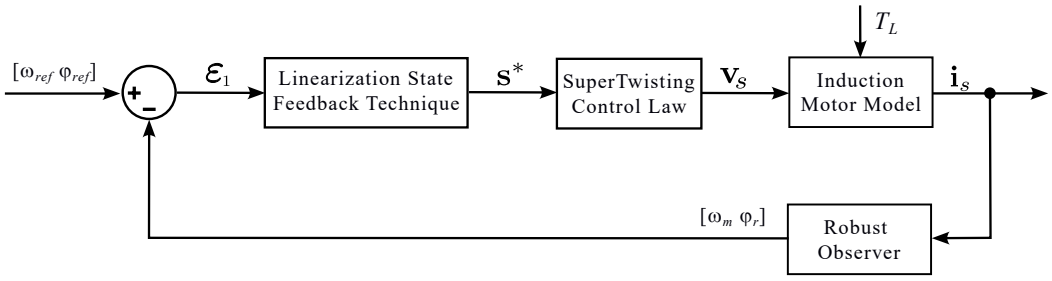


Figure 1. Schematic of the induction motor sensorless speed controller.

3. Induction Motor Model

The induction motor is a robust machine of simple construction, with acceptable speed regulation. The motor is magnetized by both the stator winding and the rotor winding by electromagnetic induction. The squirrel-cage induction motor model at the $\alpha\beta$ frame takes the following form:

$$\begin{aligned}\frac{d\omega_m}{dt} &= K_T \boldsymbol{\lambda}_r^\top \begin{bmatrix} 0 & 1 \\ -1 & 0 \end{bmatrix} \mathbf{i}_s - \frac{B_m}{J_m}\omega_m - \frac{1}{J_m}T_L \\ \frac{d\boldsymbol{\lambda}_r}{dt} &= \begin{bmatrix} -\frac{1}{T_r} & -\frac{P}{2}\omega_m \\ \frac{P}{2}\omega_m & -\frac{1}{T_r} \end{bmatrix} \boldsymbol{\lambda}_r + \frac{L_m}{T_r}\mathbf{i}_s \\ \frac{d\mathbf{i}_s}{dt} &= \begin{bmatrix} \frac{\delta}{T_r} & \frac{P}{2}\delta\omega_m \\ -\frac{P}{2}\delta\omega_m & \frac{\delta}{T_r} \end{bmatrix} \boldsymbol{\lambda}_r - \gamma \mathbf{i}_s + \frac{1}{\sigma L_s}\mathbf{v}_s \end{aligned} \tag{1}$$

where ω_m is the angular speed, while the rotor winding flux linkages and stator winding current and voltage vectors, respectively, are described by

$$\boldsymbol{\lambda}_\mathrm{r} = \begin{bmatrix} \lambda_{\alpha\mathrm{r}} & \lambda_{\beta\mathrm{r}} \end{bmatrix}^\top, \quad \mathbf{i}_\mathrm{s} = \begin{bmatrix} i_{\alpha\mathrm{s}} & i_{\beta\mathrm{s}} \end{bmatrix}^\top, \quad \mathbf{v}_\mathrm{s} = \begin{bmatrix} v_{\alpha\mathrm{s}} & v_{\beta\mathrm{s}} \end{bmatrix}^\top,$$

where term T_L is the load torque (a mechanical external input), which is considered as a disturbance for the induction motor model, and the parameter constants are

$$K_\mathrm{T} = \frac{3PL_\mathrm{m}}{4J_\mathrm{m}L_\mathrm{r}}, \quad \sigma = 1 - \frac{L_\mathrm{m}^2}{L_\mathrm{s}L_\mathrm{r}}, \quad \delta = \frac{1-\sigma}{\sigma L_\mathrm{m}},$$

$$\gamma = \frac{1}{\sigma T_\mathrm{s}} + \frac{1-\sigma}{\sigma T_\mathrm{r}}, \quad T_\mathrm{r} = \frac{L_\mathrm{r}}{R_\mathrm{r}}, \quad T_s = \frac{L_s}{R_s},$$

with P being the pole pairs, B_m is the coefficient of friction of the support points in the shaft train, J_m is the moment of inertia of the shaft train, R_r and R_s are the rotor and stator resistances, respectively, and finally, L_s, L_r, and L_m are inductance parameters defined in the process of establishing the induction motor model according to the theory of magnetically coupled circuits. The definition of these inductances is presented in the following subsection.

3.1. Definition of Induction Motor Model Inductances

The physical interpretation of the inductance parameters in the state-space model of the induction motor is crucial to avoid numerical errors when there is dependence on these parameters during the design of a state observer or the synthesis of the control system. The model's inductances (1) have the following definitions

$$L_s = L_{ss} - L_{sm} \tag{2}$$

$$L_r = L_{rr} - L_{rm} \tag{3}$$

$$L_m = \frac{3}{2}L_{srm} \tag{4}$$

where L_{ss} is the stator self-inductance per-phase, L_{sm} is the stator mutual inductance between two phases, L_{rr} is the rotor self-inductance per-phase, L_{rm} is the rotor mutual-inductance between two phases, and L_{srm} is the maximum value of the mutual inductance between stator and rotor winding.

The relations between the inductances of the equivalent circuit in **T** and the inductances of the induction motor model (2)–(4) are defined in [21], as follows:

$$L_{ls} = L_{ss} - aL_{srm} \tag{5}$$

$$L'_{lr} = a^2 L_{rr} - aL_{srm} \tag{6}$$

$$L_{mag} = aL_{srm} \tag{7}$$

where a is the ratio of turns between the stator and rotor winding per-phase; for the squirrel-cage induction motor this parameter can be considered as $a = 1$; L_{ls} is the leakage inductance of the stator, L_{mag} is the magnetizing inductance, and L_{lr} is the leakage inductance of the rotor referred to the stator side.

Accordingly, substituting (5)–(7) in (2)–(4), and considering the mutual inductance between any two stator phases as $L_{sm} = -\frac{1}{2}L_{mag}$ and any two rotor phases as $L_{rm} = -\frac{1}{2}L_{mag}$ [22], the following relations are obtained [21]:

$$L_s = L_{ls} + \frac{3}{2}L_{mag} \tag{8}$$

$$L_r = L'_{lr} + \frac{3}{2}L_{mag} \tag{9}$$

$$L_m = \frac{3}{2}L_{mag}. \tag{10}$$

Equations (8)–(10) define the inductance parameters used in the squirrel-cage induction motor model (1) in terms of the standard inductance parameters obtained from the no-load and blocked-rotor tests of the induction motor.

3.2. Adjustment of the Leakage Reactances and Stator Resistance

Once the reactance and resistance parameters of the induction motor have been determined through no-load and locked-rotor tests, it is suggested to adjust the values of the leakage reactances according to the type of squirrel-cage rotor and the rotor resistance to consider the skin effect when conducting alternating currents. The process consists of comparing the complex power, measured in the laboratory, of the motor under nominal load conditions and the complex power calculated through the equivalent circuit in T, under the same operating conditions. To obtain approximate values for power consumption in the analytical part with respect to the experimental part, a parametric analysis is performed on the stator resistance and on the percentage of each leakage reactance with respect to the reactance of the locked rotor test. The analysis stops when the complex power values are very similar.

4. Speed Control System Design for the Squirrel-Cage Induction Motor

Based on the motor model, the state-feedback speed control scheme can be synthesized; nonetheless, an observer will be needed for estimating the load torque and the variables of speed and the rotor flux linkages, as given in Section 5. As part of the control design, a state-feedback linearization mechanism is used to transform the motor model to the controllable canonical form via the definition of an error variable, which converts the problem of regulating the variables to a desired point into the stabilization of the error. The $\alpha\beta$ induction motor model (1) is a nonlinear system, which contains two electrical inputs to be determined to supply voltages to the stator winding, $v_{\alpha s}$ and $v_{\beta s}$. As a consequence, two output variables, in this case, the angular speed ω_{m} and the squared modulus of rotor flux linkages φ_{r}, can be controlled at a desired value.

For the state-feedback linearization, the following error vector is defined as

$$\boldsymbol{\varepsilon}_1 = \begin{bmatrix} \omega_{\text{ref}} - \omega_{\text{m}} \\ \varphi_{\text{ref}} - \varphi_{\text{r}} \end{bmatrix} \tag{11}$$

where

$$\varphi_{\text{ref}} = L_m \boldsymbol{\lambda}_r \mathbf{i}_{\text{s}} \tag{12}$$

and ω_{ref} are the reference set points to be followed by the output variables, and

$$\varphi_{\text{r}} = \mid \boldsymbol{\lambda}_{\text{r}} \mid^2 = \lambda_{\alpha\text{r}}^2 + \lambda_{\beta\text{r}}^2. \tag{13}$$

Based on (11) a second error variable is defined as

$$\boldsymbol{\varepsilon}_2 = \dot{\boldsymbol{\varepsilon}}_1 \tag{14}$$

and by employing the time derivative of (11), which takes into account the motor model (1), the following is obtained:

$$\boldsymbol{\varepsilon}_2 = \begin{bmatrix} \dot{\omega}_{\text{ref}} + \frac{B_{\text{m}}}{J_{\text{m}}}\omega_{\text{m}} + \frac{1}{J_{\text{m}}}T_{\text{L}} \\ \dot{\varphi}_{\text{ref}} + \frac{2}{T_{\text{r}}}\varphi_{\text{r}} \end{bmatrix} - \begin{bmatrix} K_{\text{T}}\boldsymbol{\lambda}_{\text{r}}^{\top}\mathbf{M} \\ 2\frac{L_{\text{m}}}{T_{\text{r}}}\boldsymbol{\lambda}_{\text{r}}^{\top} \end{bmatrix} \mathbf{i}_{\text{s}}. \tag{15}$$

By calculating the dynamics of $\boldsymbol{\varepsilon}_2$, the induction motor model (1) is replaced in (15), yielding the following:

$$\dot{\boldsymbol{\varepsilon}}_2 = \mathbf{F}_2 - \mathbf{B}_2\mathbf{v}_{\text{s}} \tag{16}$$

where

$$\begin{aligned} \mathbf{F}_2 = &\begin{bmatrix} \ddot{\omega}_{\text{ref}} + \frac{1}{J_{\text{m}}}\dot{T}_{\text{L}} - \frac{B_{\text{m}}}{J_{\text{m}}^2}T_{\text{L}} - \frac{B_{\text{m}}^2}{J_{\text{m}}^2}\omega_{\text{m}} \\ \ddot{\varphi}_{\text{ref}} - \frac{4}{T_{\text{r}}^2}\varphi_{\text{r}} \end{bmatrix} + \begin{bmatrix} K_{\text{T}}\boldsymbol{\lambda}_{\text{r}}^{\top}\mathbf{M} \\ 2\frac{L_{\text{m}}}{T_{\text{r}}}\boldsymbol{\lambda}_{\text{r}}^{\top} \end{bmatrix} \begin{bmatrix} \frac{\delta}{T_{\text{r}}} & \frac{P}{2}\delta\omega_{\text{m}} \\ -\frac{P}{2}\delta\omega_{\text{m}} & \frac{\delta}{T_{\text{r}}} \end{bmatrix} \boldsymbol{\lambda}_{\text{r}} \\ &- \begin{bmatrix} K_{\text{T}}\left(\frac{B_{\text{m}}}{J_{\text{m}}} - \frac{L_{\text{m}}}{T_{\text{r}}}\right)\boldsymbol{\lambda}_r^{\top}\mathbf{M} - K_{\text{T}}\dot{\boldsymbol{\lambda}}_{\text{r}}^{\top}\mathbf{M} \\ 2\frac{L_{\text{m}}}{T_{\text{r}}^2}(2 - L_{\text{m}})\boldsymbol{\lambda}_{\text{r}}^{\top} - 2\frac{L_{\text{m}}}{T_{\text{r}}}\dot{\boldsymbol{\lambda}}_{\text{r}}^{\top} \end{bmatrix} \mathbf{i}_s \end{aligned} \tag{17}$$

$$\mathbf{B}_2 = \frac{1}{\sigma T_{\text{r}} L_{\text{s}}} \begin{bmatrix} -K_{\text{T}}T_{\text{r}}\lambda_{\beta\text{r}} & K_{\text{T}}T_{\text{r}}\lambda_{\alpha\text{r}} \\ 2L_{\text{m}}\lambda_{\alpha\text{r}} & 2L_{\text{m}}\lambda_{\beta\text{r}} \end{bmatrix} \tag{18}$$

$\mathbf{v}_{\text{s}} = \begin{bmatrix} v_{\alpha\text{s}} & v_{\beta\text{s}} \end{bmatrix}^{\top}$. From (14) and (16), the following canonical representation is obtained

$$\begin{aligned} \dot{\boldsymbol{\varepsilon}}_1 &= \boldsymbol{\varepsilon}_2 \\ \dot{\boldsymbol{\varepsilon}}_2 &= \mathbf{F}_2 - \mathbf{B}_2\mathbf{v}_{\text{s}}. \end{aligned} \tag{19}$$

The transformed system (19) dynamically behaves as the motor model (1), and for the synthesis of a robust controller, the following variable is designed:

$$\mathbf{s} = \mathbf{C}_1\boldsymbol{\varepsilon}_1 + \boldsymbol{\varepsilon}_2 \tag{20}$$

where a diagonal matrix C_1 is selected to define the convergence rate of the error variables. The dynamics of (20) results in

$$\dot{\mathbf{s}} = \mathbf{C}_1\boldsymbol{\varepsilon}_2 + \mathbf{F}_2 - \mathbf{B}_2\mathbf{v}_{\text{s}}. \tag{21}$$

Nonetheless, system (21) has coupled the input $\mathbf{v}_s$ to the rotor flux linkages, as noted in (16) and (18). Thus, a decoupling, and in addition an order reduction, is achieved by proposing the following transformation:

$$\mathbf{s}^* = \mathbf{B}_2^{-1}\mathbf{s} \tag{22}$$

whose dynamics becomes

$$\dot{\mathbf{s}}^* = \mathbf{F}_2^* - \mathbf{v}_{\text{s}} \tag{23}$$

with

$$\mathbf{F}_2^* = \dot{\mathbf{B}}_2^{-1}\mathbf{B}_2\mathbf{s}^* + \mathbf{B}_2^{-1}\mathbf{C}_1\boldsymbol{\varepsilon}_2 + \mathbf{B}_2^{-1}\mathbf{F}_2.$$

Finally, the super-twisting control scheme is applied to the new decoupled system (23), yielding the closed-loop system

$$\begin{aligned} \dot{\mathbf{s}}^* &= \mathbf{F}_2^* - \boldsymbol{\lambda}|\mathbf{s}^*|^{\frac{1}{2}}\text{sign}(\mathbf{s}^*) + \mathbf{v} \\ \dot{\mathbf{v}} &= -\boldsymbol{\sigma}\ \text{sign}(\mathbf{s}^*) \end{aligned} \tag{24}$$

where $\boldsymbol{\lambda}$ and $\boldsymbol{\sigma}$ are diagonal matrices whose entries have high enough values to force the motion of the sliding variables $\mathbf{s}^*$ (22) and its time derivative $\dot{\mathbf{s}}^*$ (23) to zero. As a consequence, the sliding variable $\mathbf{s}$ in (20) reaches the origin in finite time, and thus an asymptotic motion to zero is ensured for the error variables of the speed and the squared modulus of the rotor flux linkages.

The stability analysis for (24) can be analyzed by presenting the system in the following scalar form:

$$\begin{aligned} \dot{s}_i &= -\lambda_i\ |s_i|^{\frac{1}{2}}\text{sign}(s_i) + v_i + f_i \\ \dot{v}_i &= -\sigma_i\ \text{sign}(s_i), \qquad i = \alpha, \beta. \end{aligned} \tag{25}$$

Then, a new variable is defined to obtain a dynamical system, which is appropriate for the stability analysis [20]:

$$\zeta_i = \begin{bmatrix} |s_i|^{\frac{1}{2}}\text{sign}(s_i) & v_i \end{bmatrix}^\top, \qquad |\zeta_{i1}| = |s_i|^{\frac{1}{2}}, \qquad i = \alpha, \beta, \tag{26}$$

where its time derivative results in

$$\dot{\zeta}_i = \frac{1}{|\zeta_{i1}|}\begin{bmatrix} \frac{1}{2}(-\lambda_i\zeta_{i1} + \zeta_{i2} + f_i) & -\sigma_i\zeta_{i1} \end{bmatrix}^\top. \tag{27}$$

System (27) can be expressed as the following perturbed system:

$$\dot{\boldsymbol{\zeta}}_i = \mathbf{A}_i\boldsymbol{\zeta}_i + \boldsymbol{\rho}_i \tag{28}$$

where $\mathbf{A}_i = \frac{1}{|\zeta_{i1}|}\begin{bmatrix} -\frac{1}{2}\lambda_i & \frac{1}{2} \\ -\sigma_i & 0 \end{bmatrix}$, $\boldsymbol{\rho}_i = \begin{bmatrix} \frac{1}{2|\zeta_{i1}|}f_i \\ 0 \end{bmatrix}$, $|\zeta_{i1}| = |s_i|^{\frac{1}{2}}$, and function f_i is bounded by the following restrictions:

$$|f_i| \leq \delta_i|s_i|^{\frac{1}{2}}, \ \ |f_i| \leq \delta_i|\zeta_{i1}|, \ \ 0 \leq \delta_i\ . \tag{29}$$

The stability of system (28) comes from using a candidate Lyapunov function as follows [23]:

$$V_i(\boldsymbol{\zeta}_i) = \boldsymbol{\zeta}_i^\top\mathbf{P}_i\boldsymbol{\zeta}_i \tag{30}$$

where

$$\mathbf{P}_i = \frac{1}{2}\begin{bmatrix} 4\sigma_i + \lambda_i^2 & -\lambda_i \\ -\lambda_i & 2 \end{bmatrix}.$$

Deriving in time the function (31) along the trajectories of the system, it results in

$$\dot{V}_i(\boldsymbol{\zeta}_i) = \boldsymbol{\zeta}_i^\top\left(\mathbf{A}_i^\top\mathbf{P}_i + \mathbf{P}_i\mathbf{A}_i\right)\boldsymbol{\zeta}_i + 2\boldsymbol{\zeta}_i^\top\mathbf{P}_i\boldsymbol{\rho}_i\ . \tag{31}$$

Assuming that f_i in (25) is an external disturbance bounded by

$$f_i = \delta_i |s_i|^{\frac{1}{2}} \text{sign}(s_i) = \delta_i \zeta_{i1} \,. \tag{32}$$

Involving (32) in the term $\boldsymbol{\rho}_i$ of (31) yields the following [20]:

$$\dot{V}_i(\boldsymbol{\zeta}_i) = -\frac{1}{|\zeta_{1i}|} \boldsymbol{\zeta}_i^\top \mathbf{Q}_i \boldsymbol{\zeta}_i \tag{33}$$

where

$$\mathbf{Q}_i = \frac{\lambda_i}{2} \begin{bmatrix} 2\sigma_i + \lambda_i^2 & -\left(\lambda_i - \frac{1}{2}\delta_i\right) \\ -\left(\lambda_i - \frac{1}{2}\delta_i\right) & 1 \end{bmatrix}.$$

The matrix $\mathbf{Q}_i$ must be positive definite, then λ_i and σ_i values must fulfill the following conditions:

$$\begin{aligned} &\lambda_i > 2\delta_i \\ &\sigma_i > \frac{1}{8} \frac{\lambda_i}{\lambda_i - 2\delta_i} \delta_i^2 \quad i = \alpha, \beta \end{aligned} \tag{34}$$

and the time derivative of system (33) is then negative definite, ensuring the asymptotic system stability. Inequalities (34) provide a finite time attractively sliding-mode condition on the set $s^* = 0$ and $\dot{s}^* = 0$, and as a consequence, an asymptotic movement of the tracking error variable $\boldsymbol{\varepsilon}_1$ is achieved.

5. Rotor Speed and Rotor Flux Linkages Observer Synthesis

The sensorless control scheme refers to implementing a speed motor control without the mechanical measurements, specifically the speed and the load torque; therefore, these variables need to be estimated. Additionally, the rotor flux linkages and stator currents are estimated through an observer, which converges based on the current estimation error. To this end, the rotor flux and speed observer synthesis are based on the electrical model of the induction motor (1) in the $\alpha\beta$ frame, as follows:

$$\begin{aligned} \frac{d\hat{\lambda}_\alpha}{dt} &= -\frac{1}{T_r}\hat{\lambda}_\alpha - \frac{P}{2}\hat{\omega}_m\hat{\lambda}_\beta + \frac{L_m}{T_r}\hat{i}_\alpha + C\hat{\lambda}_\beta u \\ \frac{d\hat{\lambda}_\beta}{dt} &= \frac{P}{2}\hat{\omega}_m\hat{\lambda}_\alpha - \frac{1}{T_r}\hat{\lambda}_\beta + \frac{L_m}{T_r}\hat{i}_\beta - C\hat{\lambda}_\alpha u \\ \frac{d\hat{i}_\alpha}{dt} &= \frac{\delta}{T_r}\hat{\lambda}_\alpha + \frac{P}{2}\delta\hat{\omega}_m\hat{\lambda}_\beta + \frac{L_m}{T_r}\hat{i}_\alpha + \frac{1}{\sigma L_s}v_\alpha - \frac{P}{2}\delta\hat{\lambda}_\alpha u \\ \frac{d\hat{i}_\beta}{dt} &= -\frac{P}{2}\delta\hat{\omega}_m\hat{\lambda}_\alpha + \frac{\delta}{T_r}\hat{\lambda}_\beta + \frac{L_m}{T_r}\hat{i}_\beta + \frac{1}{\sigma L_s}v_\beta - \frac{P}{2}\delta\hat{\lambda}_\beta u \end{aligned} \tag{35}$$

where $\hat{\lambda}_\alpha$, $\hat{\lambda}_\beta$ are the estimated rotor flux linkages and $\hat{i}_\alpha$, $\hat{i}_\beta$ are the estimated stator currents; parameter C is an observer adjustment constant, where $C > 0$.

The estimate of rotor flux leakages and stator currents in the $\alpha\beta$ frame is made through the following first-order sliding-mode input:

$$u = \text{U}_0 \text{sign}(s_u) \tag{36}$$

where U_0 is an observer gain, and the nonlinear sliding function s_u is defined as follows [13]:

$$s_u = (\hat{i}_\alpha - i_\alpha)\hat{\lambda}_\alpha + (\hat{i}_\beta - i_\beta)\hat{\lambda}_\beta. \tag{37}$$

As demonstrated in [13], the rotor flux observer convergence depends on the definition of the nonlinear function s_u given in (37) as an argument for the discontinuous input of the first-order sliding modes (36). The details of stability analysis can be revised in [13]. Meanwhile, the estimate of the rotor speed $\hat{\omega}_m$ is made through quasi-continuous input using the super-twisting algorithm, as follows:

$$\begin{aligned} \hat{\omega}_m &= \lambda_\omega |s_\omega|^{1/2} \text{sign}(s_\omega) + \omega_1 \\ \dot{\omega}_1 &= \alpha_\omega \, \text{sign}(s_\omega) \end{aligned} \tag{38}$$

where λ_ω and α_ω are the observer gains, while s_ω is a nonlinear sliding function, which is defined as follows [13]:

$$s_\omega = (\hat{i}_\beta - i_\beta)\hat{\lambda}_\alpha - (\hat{i}_\alpha - i_\alpha)\hat{\lambda}_\beta. \tag{39}$$

The observation convergence is achieved through the observation error of the stator currents in (37) and (39), as demonstrated in [13].

6. Robust Differentiator

For a given deterministic expression $f_0(t)$, which evolves over time, it is of interest to obtain its time derivative through a robust differentiator. The numerical differentiation becomes robust against mathematically known $f_0(t)$ and only requires the upper bound to be used as a Lipschitz constant of the derivative $L > 0$ [19,24]. Hence, the differentiator obtains an estimation in real-time of $f_0(t)$ and its time derivative $\dot{f}_0(t)$.

The robust differentiator is given as

$$\begin{aligned} \dot{z} = v &= -\lambda_1 \mid z - f_0(t) \mid^{\frac{1}{2}} \text{sign}(z - f_0(t)) + z_1 \\ \dot{z}_1 &= -\lambda_2 \text{sign}(z - f_0(t)) \end{aligned} \tag{40}$$

where the state variable z converges to $f_0(t)$, while v (or z_1) becomes the time derivative of $f_0(t)$, that is $\dot{f}_0(t)$ [24]. The robust differentiator convergence is formerly demonstrated in [24], which closely follows the super-twisting controller proof, where the convergence depends on appropriately selecting the large values of the gains λ_1 and λ_2 and by fulfilling the following conditions:

$$L < \lambda_2 \qquad \text{and} \qquad \frac{2(\lambda_2 + L)^2}{\lambda_1^2(\lambda_2 - L)} < 1. \tag{41}$$

7. Results

The real-time sensorless rotor speed controller runs on a dSPACE 1103 Control Board kit (Paderborn, Germany) interfaced with LabVolt academic equipment (Québec, QC, Canada), with algorithms implemented in MATLAB/Simulink, version 2011b. The results were obtained on a test bench comprising a 260 V DC bus from the power supply, which feeds a three-phase bridge-type inverter operating at a switching frequency of 4.68 kHz. The inverter supplies a controlled voltage $\mathbf{v}_s$ to a squirrel-cage induction motor mechanically coupled to a dynamometer via a toothed belt. The base program was configured in MATLAB/Simulink using a fixed-step solver with a 100 µs time step and was compiled for the dSPACE DS1103 control board. The rotor speed controller takes the stator current $\mathbf{i}_s$ as its only input and generates a control signal $\mathbf{u}_s$ as output, which is conditioned to activate the inverter. To generate the control signal, the system estimates both the rotor speed and the rotor flux linkage and calculates the argument of the control law by applying the linearization state feedback technique. Additionally, the system configures the load torque of the dynamometer and sends it through an analog output. Figure 2 shows the schematic

of the induction motor speed control system. The induction motor nameplate data are as follows: 175 W, 120 V, 1.5 A, and 1740 r.p.m. The parameters used in the experimental tests are presented in Table 1, which includes both the motor parameters and the gains for tuning the controller and the gains to achieve observer convergence.

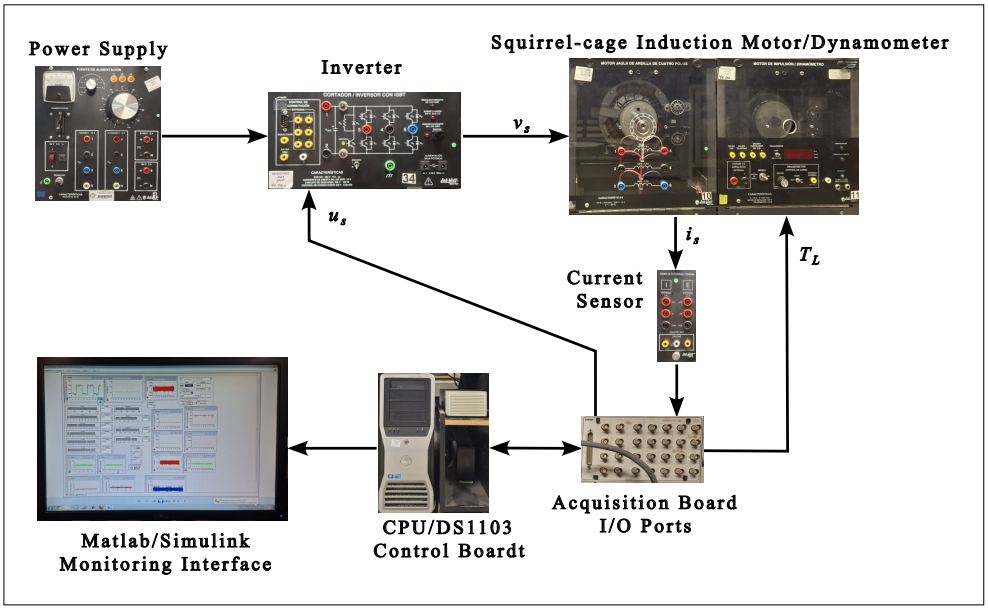


Figure 2. Schematic of the induction motor speed control system.

Table 1. Motor, controller, and observer parameters.

Motor		Controller		Observer	
Parameter	**Value**	**Parameter**	**Value**	**Parameter**	**Value**
R_s	13.7 Ω	λ_α	160	λ_ω	380
R_r	6.8 Ω	σ_α	200	α_ω	82
L_s	0.7 H	λ_β	120	C	3.8
L_r	0.69 H	σ_β	730	U_0	3.0
L_m	0.66 H	C_{11}	700		
P	4 poles	C_{22}	840		
J_m	0.0037				
B_m	0.0033				

Two laboratory experiments were conducted to validate the proposed sensorless rotor speed control system. The first experiment assessed the observer's capability to estimate rotor speed and rotor flux linkages under external disturbances such as sudden load-torque steps and supply-voltage fluctuations. The second experiment evaluated the closed-loop sensorless speed controller under external disturbances.

7.1. Rotor Speed Observer Performance

Using the robust observer (35), both rotor speed and rotor flux linkages are simultaneously estimated. Figure 3 depicts the rotor speed estimation performance of the observer under external disturbances. A load-torque pulse train with a 0.5 N·m amplitude, 4 s pulse, and 8 s period was applied. Simultaneously, the supply voltage amplitude is varied from 150 to 170 V with a pulse train phase-shifted by 2 s with respect to the load-torque pulse train, see Figure 3a,b. Rotor speed estimation remains highly accurate under varying external disturbances, as shown in Figure 3c.

The observer's performance in estimating the rotor flux linkages based on the observation of currents in the α-β reference frame is shown in Figure 4. The estimated current

closely follows the measured current on both the α and β axes, as illustrated in Figure 4a and Figure 4b, respectively. Thereby, the rotor flux linkages are estimates, with a maximum value of approximately 0.35 Wb-turn and are 90 degrees out of phase with each other.

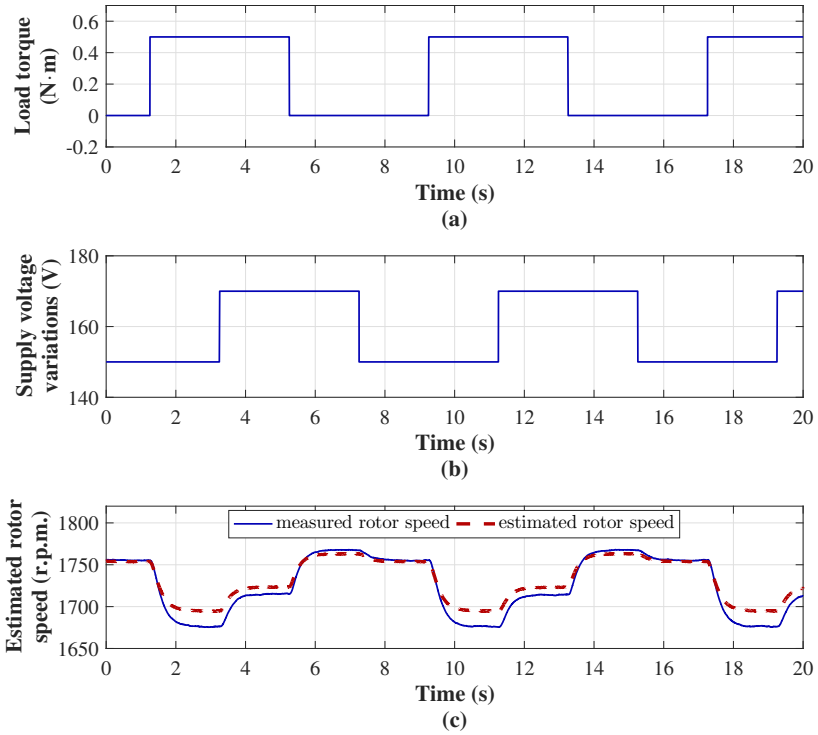


Figure 3. Observer performance in estimating rotor speed. (**a**) Load torque disturbances; (**b**) supply voltage variations; (**c**) estimated rotor speed.

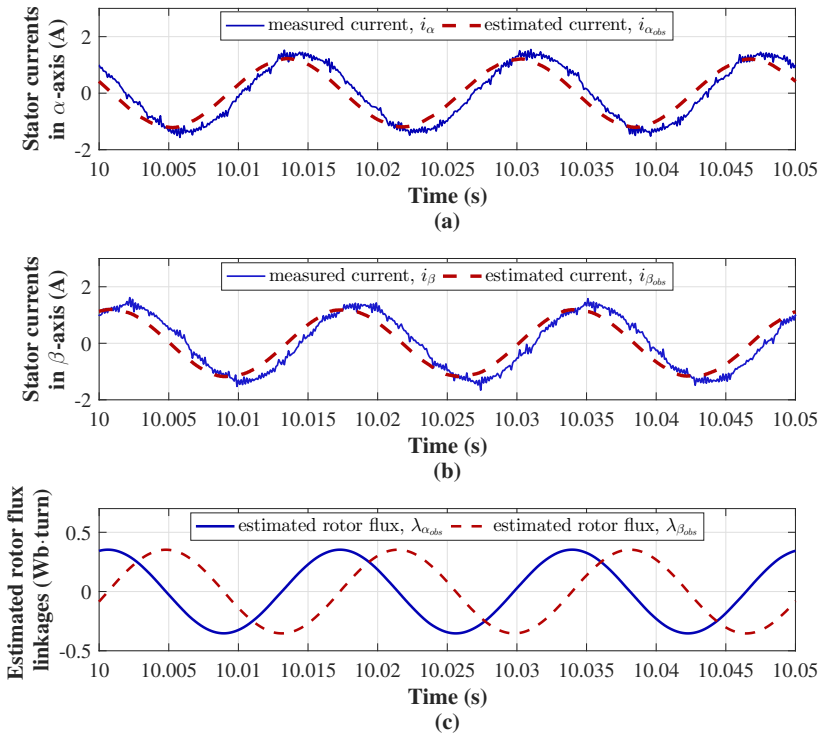


Figure 4. Observer performance in estimating rotor fluxes. (**a**) Estimated current in α-axis; (**b**) estimated current in β-axis; (**c**) estimated rotor flux linkages.

7.2. Sensorless Rotor Speed Controller Performance

The control goal of the sensorless rotor speed controller consists of the tracking of the rotor speed and the squared modulus of the rotor flux linkages with their references in the presence of changes in load torque and reference speed, as is shown in Figure 5. The load torque, as an external disturbance, is configured through a pulse train with an amplitude of 0.5 N·m, a pulse of 4 s, and a period of 8 s. Simultaneously, the speed reference varies with another pulse train phase-shifted by 2 s with respect to load-torque pulse. The speed reference oscillates between 1600 and 1700 r.p.m. every 0.8 s, and the control action forces the estimated rotor speed to closely track the reference, as shown in Figure 5b. This demonstrates that the control system of the speed tracking remains accurate despite the presence of the load-torque pulse train (Figure 5a) and sudden changes in the speed reference. Meanwhile, the squared modulus of the rotor flux linkages (13) enables precise reference tracking (12), even under simultaneous changes in load torque and speed reference, as shown in Figure 5c. Rotor flux tracking varies due to changes in the rotor flux linkages reference as the current follows changes in the load torque.

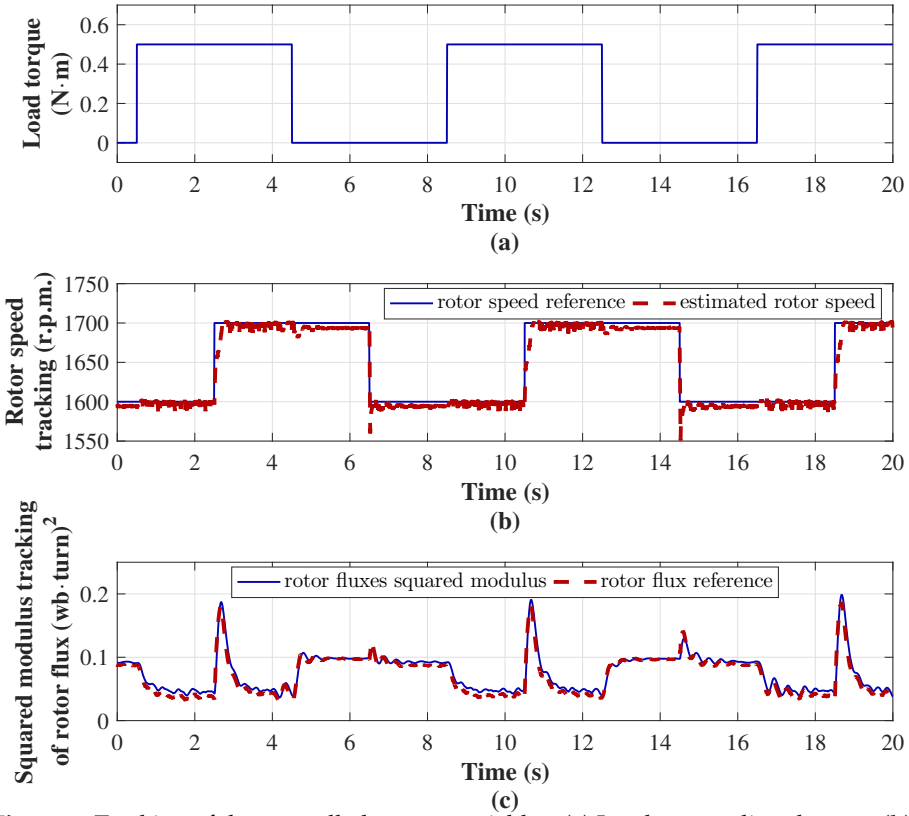


Figure 5. Tracking of the controlled output variables. (**a**) Load torque disturbances; (**b**) rotor speed tracking; (**c**) squared modulus tracking of rotor flux linkages.

The performance of the control input in the α-axis under external disturbances is shown in Figure 6. Figure 6a–d show the response to the change in the input load torque, while Figure 6e–h show the response to the change in the reference speed. A change in load torque from 0 to 0.5 N·m, applied as an external disturbance, has little effect on the control action v_α, as illustrated in Figure 6a–d. When the speed reference changes from 1600 to 1700 r.p.m. at $t = 10.51$ s (Figure 6e), the control action successfully drives the sliding variable (22) to the origin in approximately 0.2 s (Figure 6g). This ensures a smooth convergence of the speed tracking error variable (20) to zero within the same time frame (Figure 6f), fulfilling the goal of controlling the induction motor speed. The control input, interpreted as the voltage applied to the stator winding in the α-axis, is depicted in

Figure 6h. When the change in reference speed acts as an external disturbance, v_α saturates at 250 V. Since the supply source can only provide a maximum of 180 V, this limitation delays the system's transient transient response.

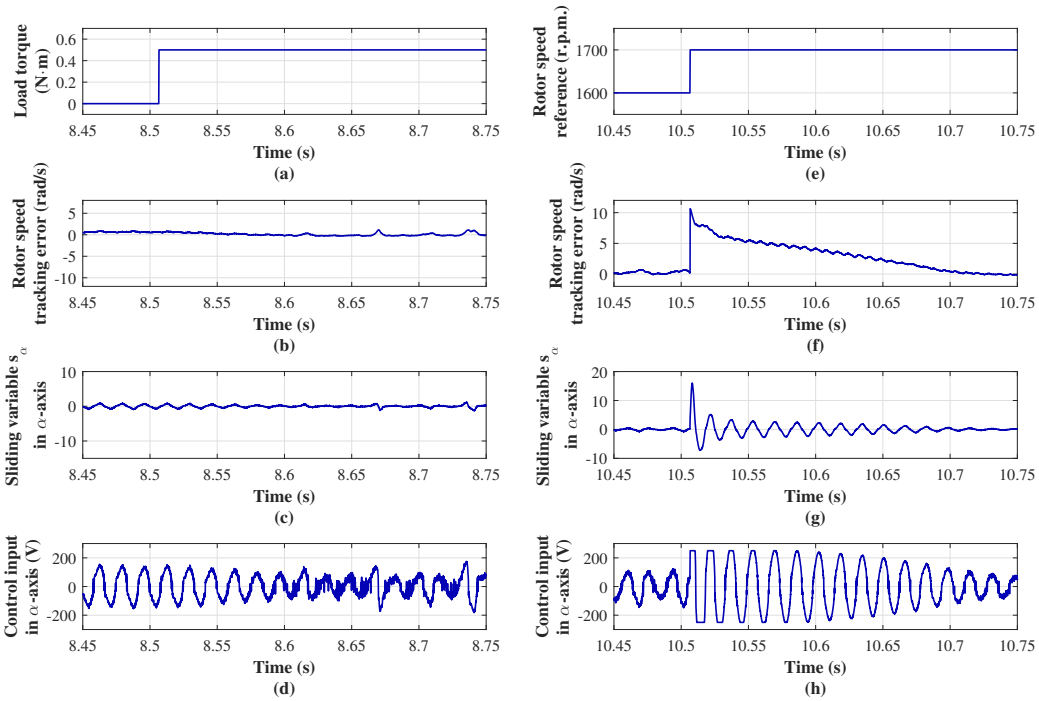


Figure 6. Performance of the control input on the α-axis. (**a**–**d**) Load torque disturbances cancellation; (**e**–**h**) control action due to sudden changes in reference speed.

The performance of the control input in the β-axis under external disturbances is presented in Figure 7. In Figure 7a–d, the load torque changes from 0 to 0.5 N·m (Figure 7a). Following this torque increase, the control action v_β forces the sliding variable to the origin (Figure 7c), leading to a smooth convergence of the flux tracking error to zero (Figure 7b). Meanwhile, Figure 7e–h show the response to reference speed change. When the speed reference changes from 1600 to 1700 r.p.m. as an external disturbance (Figure 7e), the control input acts immediately to drive the sliding variable to zero within approximately at 0.4 s albeit with oscillatory behavior. Consequently, the tracking error of the flux squared modulus also converge smoothly to zero at 0.4 s. At the onset of the transient, the control input saturates at 250 V.

A robust observer, responsible for estimating rotor speed and flux linkages, is essential for the operation of the control system. Its performance under external perturbations, such as a change in the reference speed, is illustrated in Figure 8. The estimation of the stator currents in the α-β axes is of high accuracy, see Figure 8a,b, and allows a reliable estimation of both the rotor flux links and the rotor speed. When a disturbance occurs due to a sudden change in the reference speed from 1600 to 1700 r.p.m. at $t = 10.51$ s, oscillations appear in the estimated rotor flux links (Figure 8c). Finally, the estimated rotor speed converges to the measured rotor speed in the time range of 0.26 s, see Figure 8d.

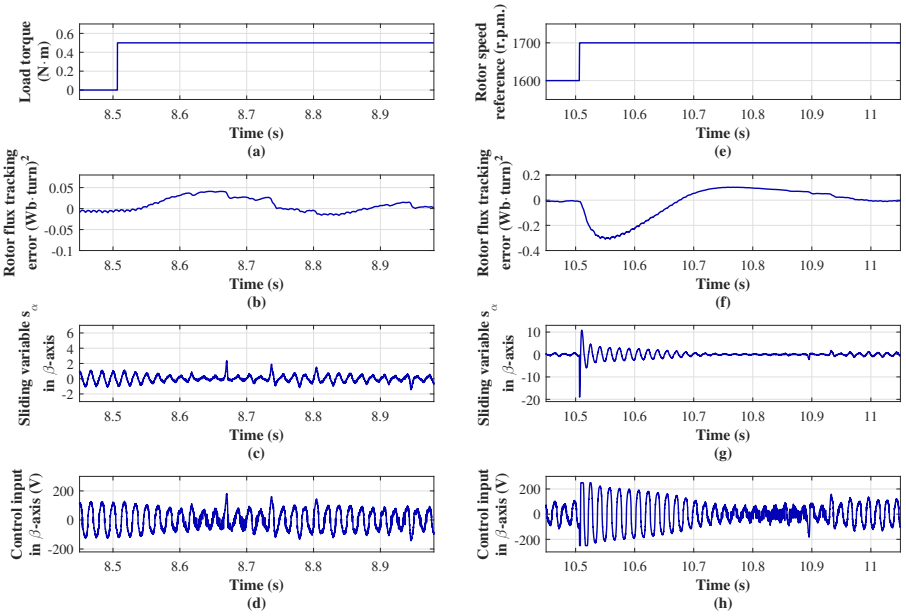


Figure 7. Performance of the control input on the β-axis. (**a**–**d**) Load torque disturbances cancellation; (**e**–**h**) control action due to sudden changes in reference speed.

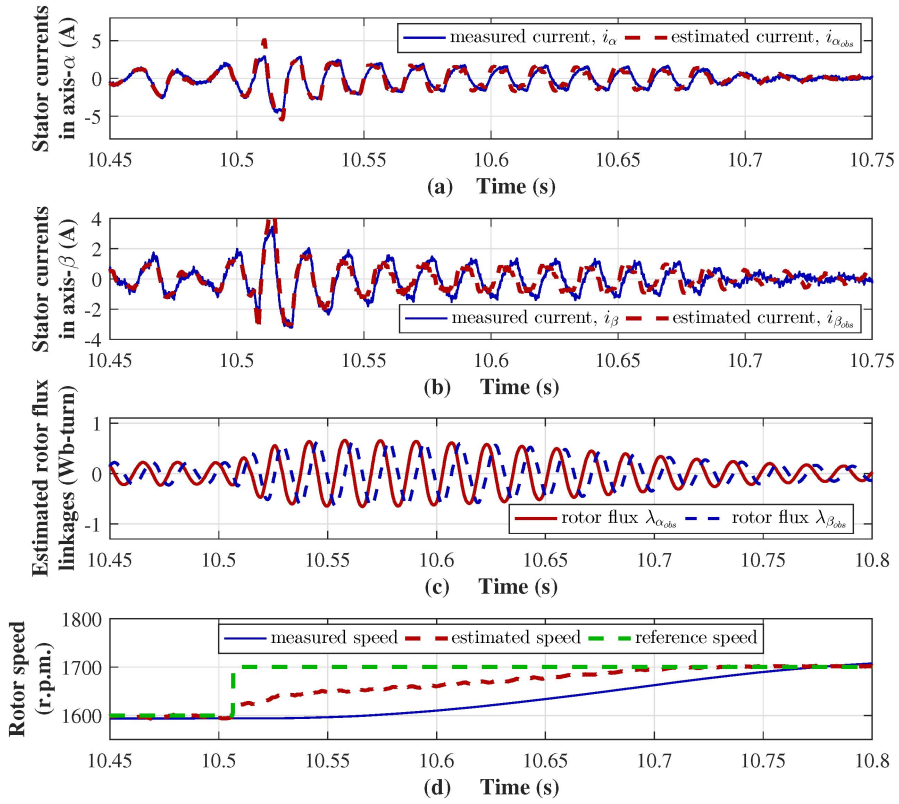


Figure 8. Observer performance in the sensorless rotor speed controller. (**a**) Estimated current in α-axis; (**b**) estimated current in β-axis; (**c**) estimated rotor flux linkages; (**d**) estimated rotor speed.

8. Conclusions

In this work, a robust speed control system for the induction motor, which eliminates the need for mechanical sensors, is presented. Its performance is validated through experimental testing, demonstrating robust operation under varying load torques and reference speed changes. The proposed control system utilizes the sliding-mode super-twisting

control law, which forces the sliding variable to move towards the origin in finite time, thereby asymptotically decaying the error variable to zero. With this, the rotor speed and the modulus of the rotor flux linkages reach their references. It is essential to highlight one of the contributions of this work, which consists of the reference function of the rotor flux module, which automatically adjusts with changes in stator currents, because of the motor operating conditions. Simultaneous estimation of rotor speed and rotor flux linkages is carried out using a robust observer based on sliding modes. A first-order sliding-mode input steers a nonlinear sliding function toward the origin. At the same time, a super-twisting sliding-mode input forces a second nonlinear sliding function towards zero. This is to achieve convergence of the estimated rotor speed and flux linkages. This combination represents a novel contribution by enabling finite-time convergence of both rotor speed and squared rotor flux magnitude while ensuring smooth transient behavior. These results confirm the effectiveness of the proposed control and observation strategy for induction motor drives. Finally, the results confirm its practical applicability beyond laboratory settings. By bridging robust nonlinear control theory and practical implementation in induction motor drives, this work advances the research line on finite-time sensorless control, providing a reproducible framework that other researchers and practitioners can adopt, refine, and extend.

Author Contributions: Synthesis process of the speed observer, speed control system, and robust differentiator, O.M. and F.O.-T.; definition of the induction motor model and definition of inductance parameters, O.M., N.P., O.H., and F.V.; experimentation to validate the proposal, O.M., O.H., and M.G.; formal analysis, O.M., F.O.-T., and R.R.-B.; investigation, M.G. and F.O.-T.; writing—original draft preparation, O.M., and F.V.; writing—review and editing, M.G., F.O.-T., R.R.-B., N.P., and O.M.; project administration, O.M.; funding acquisition, O.M., N.P., and F.O.-T. All authors have read and agreed to the published version of this manuscript.

Funding: This research was partially funded by Universidad Autónoma de Ciudad Juárez (UACJ) through the Call for Research Projects with Social Impact (PIISO) in 2023 grant number PIISO23-IIT-13-OAMORFIN, and the Coordination of Scientific Research (period 2025) of the Universidad Michoacana de San Nicolás de Hidalgo (UMSNH).

Data Availability Statement: The original contributions presented in this study are included in the article. Further inquiries can be directed to the corresponding authors.

Acknowledgments: We gratefully acknowledge the administrative and support staff of the Electrical Engineering Laboratory in the Department of Electrical Engineering and Computer Science at the Institute of Engineering and Technology, Universidad Autónoma de Ciudad Juárez, for their invaluable assistance during the experimental work with the LabVolt academic equipment, which significantly contributed to the success of this research.

Conflicts of Interest: The authors declare no conflict of interest.

References

1. Benaicha, S. Robust Sensorless Speed Control of an Induction Motor Drive Using a Synergetic Approach. *Rev. Roum. Des Sci. Tech. Sér. Électrotech. Énergétique* **2023**, *68*, 381–387. [CrossRef]
2. El Daoudi, S.; Lazrak, L.; Ait, L. Sliding mode approach applied to sensorless direct torque control of cage asynchronous motor via multi-level inverter. *Prot. Control Mod. Power Syst.* **2020**, *5*, 1–10. [CrossRef]
3. Mencou, S.; Yakhlef, M.B.; Tazi, E.B. Advanced Torque and Speed Control Techniques for Induction Motor Drives: A Review. In Proceedings of the 2022 2nd International Conference on Innovative Research in Applied Science, Engineering and Technology (IRASET), Meknes, Morocco, 3–4 March 2022; pp. 1–9. [CrossRef]
4. Halimi, H.; Elgarouaz, M.; Lazrak, L.; El Daoudi, S. Robustness and high performances of sensorless induction motor with combined backstepping command and high order sliding mode control. *Int. J. Dyn. Control* **2025**, *13*, 1123–1135. [CrossRef]
5. Hu, H.; Yu, S.; Ren, L.; Zhai, M.; Chen, Y. Improved Interconnected MRAS Parameter Identification for Speed Sensorless Control of Linear Induction Motor. *Actuators* **2025**, *14*, 2 [CrossRef]

6. Li, X.; Zhang, Y.; Wang, H.; Xu, D. Speed sensorless control employing adaptive sliding mode observer and MRAS for induction motor drives. *J. Phys. Conf. Ser.* **2020**, *1633*, 012145. [CrossRef]
7. Korzonek, M.; Tarchala, G.; Orlowska-Kowalska, T. A review on MRAS-type speed estimators for reliable and efficient induction motor drives. *ISA Trans.* **2019**, *93*, 1–13. [CrossRef] [PubMed]
8. Golsorkhi, M.S.; Binandeh, H.; Savaghebi, M. Online Efficiency Optimization and Speed Sensorless Control of Single-Phase Induction Motors. *Appl. Sci.* **2021**, *11*, 8863. [CrossRef]
9. Azab, M. A Review of Recent Trends in High-Efficiency Induction Motor Drives. *Vehicles* **2025**, *7*, 15. [CrossRef]
10. Zaky, M.S.; Metwaly, M.K. Improved MRAS observer with rotor flux correction terms and FLC-based adaptive law for sensorless induction motor drives. *Sci. Rep.* **2025**, *15*, 1–20. [CrossRef] [PubMed]
11. El Merrassi, W.; Abounada, A.; Ramzi, M. Advanced speed sensorless control strategy for induction machine based on neuro-MRAS observer. *Mater. Today Proc.* **2021**, *45*, 7615–7621. [CrossRef]
12. Cárdenas, R.; Pena, R. Sensorless vector control of induction machines for variable-speed wind energy applications. *IEEE Trans. Energy Convers.* **2004**, *19*, 196–205. [CrossRef]
13. Yan, Z.; Jin, C.; Utkin, V. Sensorless sliding-mode control of induction motors. *IEEE Trans. Ind. Electron.* **2000**, *47*, 1286–1297. [CrossRef]
14. Utkin, V.; Guldner, J.; Shi, J. *Sliding Mode Control in Electro-Mechanical Systems*; Taylor and Francis: Philadelphia, PA, USA, 1999.
15. Gadoue, S.M.; Giaouris, D.; Finch, J.W. MRAS sensorless vector control of an induction motor using new sliding-mode and fuzzy-logic adaptation mechanisms. *IEEE Trans. Energy Convers.* **2009**, *25*, 394–402. [CrossRef]
16. Benderradji, H.; Benaicha, S.; Alaoui, L.C. Improved sliding mode control for induction motor based on twisting algorithm. *AIMS Electron. Electr. Eng.* **2025**, *9*, 81–98. [CrossRef]
17. Hamdi, W.; Hammoudi, M.Y.; Betka, A. Sensorless Speed control of induction motor using model reference adaptive system and deadbeat regulator. *Eng. Proc.* **2023**, *56*, 16. [CrossRef]
18. Govindharaj, I.; Kumar, D.; Balamurugan, S.; Yazhinian, S.; Anandh, R.; Rampriya, R.; Karthick, G.; Michael, G. Sensorless vector-controlled induction motor drives: Boosting performance with adaptive neuro-fuzzy inference system integrated augmented model reference adaptive system. *MethodsX* **2024**, *13*, 102992. [CrossRef]
19. Levant, A. Higher-order sliding modes, differentiation and output-feedback control. *Int. J. Control* **2003**, *76*, 924–941. [CrossRef]
20. Dávila, A.; Moreno, J.A.; Fridman, L. Optimal Lyapunov function selection for reaching time estimation of super twisting algorithm. In Proceedings of the 48h IEEE Conference on Decision and Control (CDC) Held Jointly with 2009 28th Chinese Control Conference, Shanghai, China, 15–18 December 2009; pp. 8405–8410. [CrossRef]
21. Morfín, O.A.; Castañeda, C.E.; Ruiz-Cruz, R.; Valenzuela, F.A.; Murillo, M.A.; Quezada, A.E.; Padilla, N. The squirrel-cage induction motor model and its parameter identification via steady and dynamic tests. *Electr. Power Components Syst.* **2018**, *46*, 302–315. [CrossRef]
22. Krause, P.C.; Wasynczuk, O.; Sudhoff, S.D.; Pekarek, S. *Analysis of Electric Machinery and Drive Systems*; Wiley Online Library: Hoboken, NJ, USA, 2002; Volume 2. [CrossRef]
23. Zenteno-Torres, J.; Cieslak, J.; Dávila, J.; Henry, D. Sliding Mode Control with Application to Fault-Tolerant Control: Assessment and Open Problems. *Automation* **2021**, *2*, 1–30. [CrossRef]
24. Shtessel, Y.; Edwards, C.; Fridman, L.; Levant, A. *Sliding Mode Control and Observation*; Springer: Berlin/Heidelberg, Germany, 2014; Volume 10.

Disclaimer/Publisher's Note: The statements, opinions and data contained in all publications are solely those of the individual author(s) and contributor(s) and not of MDPI and/or the editor(s). MDPI and/or the editor(s) disclaim responsibility for any injury to people or property resulting from any ideas, methods, instructions or products referred to in the content.